Since January 2020 Elsevier has created a COVID-19 resource centre with free information in English and Mandarin on the novel coronavirus COVID-19. The COVID-19 resource centre is hosted on Elsevier Connect, the company's public news and information website.

doi:10.1016/j.jmb.2010.09.068 J. Mol. Biol. (2010) 404, 650–664

Contents lists available at www.sciencedirect.com

Journal of Molecular Biology

journal homepage: http://ees.elsevier.com.jmb

Crystal Structure of Human Interferon-λ1 in Complex with Its High-Affinity Receptor Interferon-λR1

Zachary J. Miknis[1], Eugenia Magracheva[1,2], Wei Li[3], Alexander Zdanov[1]†, Sergei V. Kotenko[3] and Alexander Wlodawer[1]*

[1]*Macromolecular Crystallography Laboratory, NCI-Frederick, Frederick, MD 21702, USA*
[2]*Basic Research Program, SAIC-Frederick, Frederick, MD 21702, USA*
[3]*Department of Biochemistry and Molecular Biology, University Hospital Cancer Center, UMDNJ-New Jersey Medical School, Newark, NJ 07103, USA*

Received 16 August 2010; received in revised form 29 September 2010; accepted 30 September 2010
Available online 8 October 2010

Edited by I. Wilson

Keywords:
cytokine;
crystallography;
antiviral;
immunity;
signaling

Interferon (IFN)-λ1 [also known as interleukin (IL)-29] belongs to the recently discovered group of type III IFNs. All type III IFNs initiate signaling processes through formation of specific heterodimeric receptor complexes consisting of IFN-λR1 and IL-10R2. We have determined the structure of human IFN-λ1 complexed with human IFN-λR1, a receptor unique to type III IFNs. The overall structure of IFN-λ1 is topologically similar to the structure of IL-10 and other members of the IL-10 family of cytokines. IFN-λR1 consists of two distinct domains having fibronectin type III topology. The ligand–receptor interface includes helix A, loop AB, and helix F on the IFN site, as well as loops primarily from the N-terminal domain and inter-domain hinge region of IFN-λR1. Composition and architecture of the interface that includes only a few direct hydrogen bonds support an idea that long-range ionic interactions between ligand and receptor govern the process of initial recognition of the molecules while hydrophobic interactions finalize it.

Published by Elsevier Ltd.

Introduction

Interferon (IFN)-λ1, IFN-λ2, and IFN-λ3 are class II cytokines[1] belonging to the recently identified group of type III IFNs.[2] These cytokines were also designated as interleukin (IL)-29, IL-28A, and IL-28B, respectively.[3] IFN-λs, together with IFN-α/β, the classical type I IFNs, serve as master regulators of a multifaceted antiviral response.[4] Antiviral activities of IFN-λs have been demonstrated against a broad variety of viruses in cell culture experiments and *in vivo*. For example, IFN-λs have been shown to inhibit infection by the hepatitis C virus (HCV) and the hepatitis B virus,[5,6] a number of respiratory viruses infecting epithelial cells (influenza A and B, respiratory syncytial virus, human metapneumovirus, and severe acute respiratory syndrome),[7] and herpes simplex virus type 2[8] and cytomegalovirus (CMV).[9]

Both type I and type III IFNs are co-produced by various nucleated cells in response to live viral infections and to a variety of stimuli (lipopolysaccharides, poly I:C, bacterial/viral DNA) triggering toll-like receptor signaling.[1] Moreover, both types of IFNs activate the same signal transduction pathways, including formation of the IFN-stimulated

*Corresponding author. E-mail address: wlodawer@nih.gov.

† Deceased.

This paper is dedicated to the memory of Dr. Alexander (Sasha) Zdanov who was leading this project until his untimely death. We will miss him.

Abbreviations used: IFN, interferon; IL, interleukin; HCV, hepatitis C virus; CMV, cytomegalovirus; EBV, Epstein–Barr virus; PEG, polyethylene glycol; PDB, Protein Data Bank; NAG, *N*-acetylglucosamine; Sc, shape complementarity; SNP, single nucleotide polymorphism.

0022-2836/$ - see front matter. Published by Elsevier Ltd.

gene factor 3 transcription complex.[2] Both types of IFNs induce expression of the same set of genes[6,10,11] and, therefore, have very similar biological activities that include strong intrinsic antiviral activity.[1]

However, whereas type I IFNs are able to activate a potent antiviral state in a wide variety of cells,[4,12] type III IFNs are primarily active on epithelial cells.[13,14] The cell-type selective action of type III IFNs is possible because each type of IFN engages its own unique receptor complex for signaling and because of the distinct expression pattern of IFN receptors. Type I IFNs signal through a common cellular IFN-α/β receptor complex composed of two unique subunits, IFN-αR1 and IFN-αR2, which are ubiquitously expressed.[12,15] However, type III IFNs signal through an IFN-λ receptor complex, which consists of a unique IFN-λR1 chain and a shared IL-10R2 chain, the latter also being the second subunit of the IL-10, IL-22, and IL-26 receptor complexes.[1] In contrast to the ubiquitously expressed IFN-α/β receptor subunits and the IL-10R2 chain, the IFN-λR1 chain is expressed primarily by epithelial cells and dendritic cells restricting action of type III IFNs to epithelial cells.[13,14] IL-10 has been shown to have low affinity for the IL-10R2 component of the receptor complex[16] and IFN-λ1 is presumed to have low affinity for IL-10R2 as well.

In addition to the well-known antiviral activity of IFN-λ, it has been demonstrated that IFN-λ may have anticancer activity as well. IFN-λs have been shown to reduce proliferation of several cancer cell lines such as the colorectal-cancer-derived HCT116 cells,[9] glioblastoma LN319 cells,[4] and aneuroendocrine BON1 tumor cells.[17] In certain esophageal cancer cell lines, it has been found that IFN-λ1 can inhibit their growth through G1 phase arrest and have enhanced antitumor effects in combination with anticancer chemotherapeutics.[18] Other agents such as IFN-γ or the proteasome inhibitor Bortezomib can augment the antiproliferative and pro-apoptotic effects of IFN-λ in cancer cells.[19,20] With the use of murine tumor models, IFN-λ has been shown to inhibit the growth of MCA205 fibrosarcoma cells *in vivo*[21] and retard or suppress the growth of B16 melanoma cells[13,22] and BNL hepatoma cells in mice.[23] These studies suggested that investigation of IFN-λ could have benefits not only for treatment of viral diseases such as chronic hepatitis C but also as a cancer chemotherapeutic. Given the more limited expression of IFN-λR1 throughout the body, it is also likely that use of IFN-λ as a treatment option would be generally tolerated better than treatment with more ubiquitously recognized IFNs, such as IFN-α and IFN-β.

All three known type III IFNs demonstrate limited amino acid similarity to both type I IFNs and IL-10-related cytokines.[1,12] On the other hand, the level of amino acid conservation is very high among members of the IFN-λ family (96% similarity between IFN-λ2 and IFN-λ3), yet the activity of IFN-λ3 and IFN-λ2 differs by 16-fold, whereas IFN-λ3 is 2-fold more active than IFN-λ1.[24] Knowledge of the structural details of the IFN-λ receptor complexes may provide insights into the differential activity of these cytokines. The known IFN and IL receptor subunits including IL-10R1 and IL-10R2 are structurally related, share a low degree of amino acid similarity in their extracellular domains (with the identity to IL-10R1 ranging from 11% to 13%), and belong to the family of class II cytokine receptors.[25,26]

Structures of several IFNs and IL-10 family members, as well as their dimeric and trimeric cytokine receptor complexes, have been elucidated by crystallography and NMR.[27–34] Structural information is available for the human and viral IL-10,[31,32] the latter from the Epstein–Barr virus (EBV) and CMV, as well as in complexes with IL-10R1.[16,35,36] IL-19 has had its structure determined in the absence of the receptor,[37] whereas IL-22 has been crystallized both alone[30,38] and in complex with IL-22R1[39,40] and IL-22BP.[41] All of the IL-10 receptor–ligand structures include a dimer of IL-10 binding to IL-10R1 in a 1:2 ratio. The ligand–receptor interface consists of residues residing on helix A, loop AB, and helix F of IL-10 and on inter-domain loops of IL-10R1, primarily stabilized by hydrophobic interactions. It has been suggested, based on the structure of IL-10 bound to IL-10R1,[35] that the receptor-binding site on IL-10 is shared by both IL-10R1 and IL-10R2. EBV IL-10 binds to IL-10R1 with 1000-fold lower affinity than IL-10 due to small changes in both EBV IL-10 positioning on IL-10R1 and inter-helix loops of EBV IL-10.[16] In contrast, CMV IL-10 exhibits affinity for IL-10R1 similar to IL-10 but differs in its inter-domain angle by 40° as compared to IL-10.[36] A model for binding of IL-10 to IL-10R1 and IL-10R2 has been proposed recently based on site-directed mutagenesis experiments,[28] updating the previously published model of the ternary IL-10/IL-10R1/IL-10R2 complex.[34] In addition, a model for the binding of CMV IL-10 to IL-10R1 and IL-10R2 has been proposed.[28]

The crystal structure of isolated IFN-λ3 has been determined recently.[29] It has shown the molecule to be a monomer highly similar to one domain of the domain-swapped IL-10 molecule, despite low sequence homology between the two proteins. Single-nucleotide polymorphisms (SNPs), some of which cause amino acid substitutions, within the type III IFN genomic locus are found in patients who spontaneously clear chronic HCV infection, as well as patients who respond well to IFN-α treatment for HCV infection.[42–46] It is unknown how these variations affect the activity of the various members of the IFN-λ family.

Following the previous report of protein production and crystallization,[47] we report here

determination and analysis of the X-ray crystal structures of IFN-λ1 (expressed in both *Escherichia coli* and *Drosophila* S2 cells) complexed with its receptor IFN-λR1 (expressed in *Drosophila* S2 cells). The structures show a 1:1 complex between monomeric IFN-λ1 and IFN-λR1, as opposed to the 1:2 complexes seen for IL-10/IL-10R1. The interface between the two proteins is highly hydrophobic in nature and the amino acid composition and bonding patterns suggest that electrostatic interactions may be responsible for initial ligand–receptor association, while hydrophobic interactions solidify the interaction. The overall folding of IFN-λ1 and IFN-λR1 are similar to other cytokines and cytokine receptors, respectively, and the complex offers hints about how subtle variations between IFN-λ1, IFN-λ2 and IFN-λ3 might influence the activity of the cytokines toward HCV.

Results

We determined the crystal structure of IFN-λ1 bound to its high-affinity receptor IFN-λR1. IFN-λ1 used in crystallization experiments was expressed both in *E. coli* cells (IFN-$\lambda1_{bac}$) and in *Drosophila* cells (IFN-$\lambda1_{ins}$), whereas IFN-λR1 was expressed only in insect cells.[47] Both complexes were formed in a 1:1 molar ratio, purified, and crystallized. The details of expression, purification, crystallization, and data collection procedures have been previously described.[47] The crystal structures were solved using molecular replacement and revealed a complex consisting of IFN-λ1 bound to IFN-λR1 in a 1:1 ratio. Since the two structures determined in this work are essentially identical with one another, only the structure of the IFN-$\lambda1_{ins}$/IFN-λR1 complex will

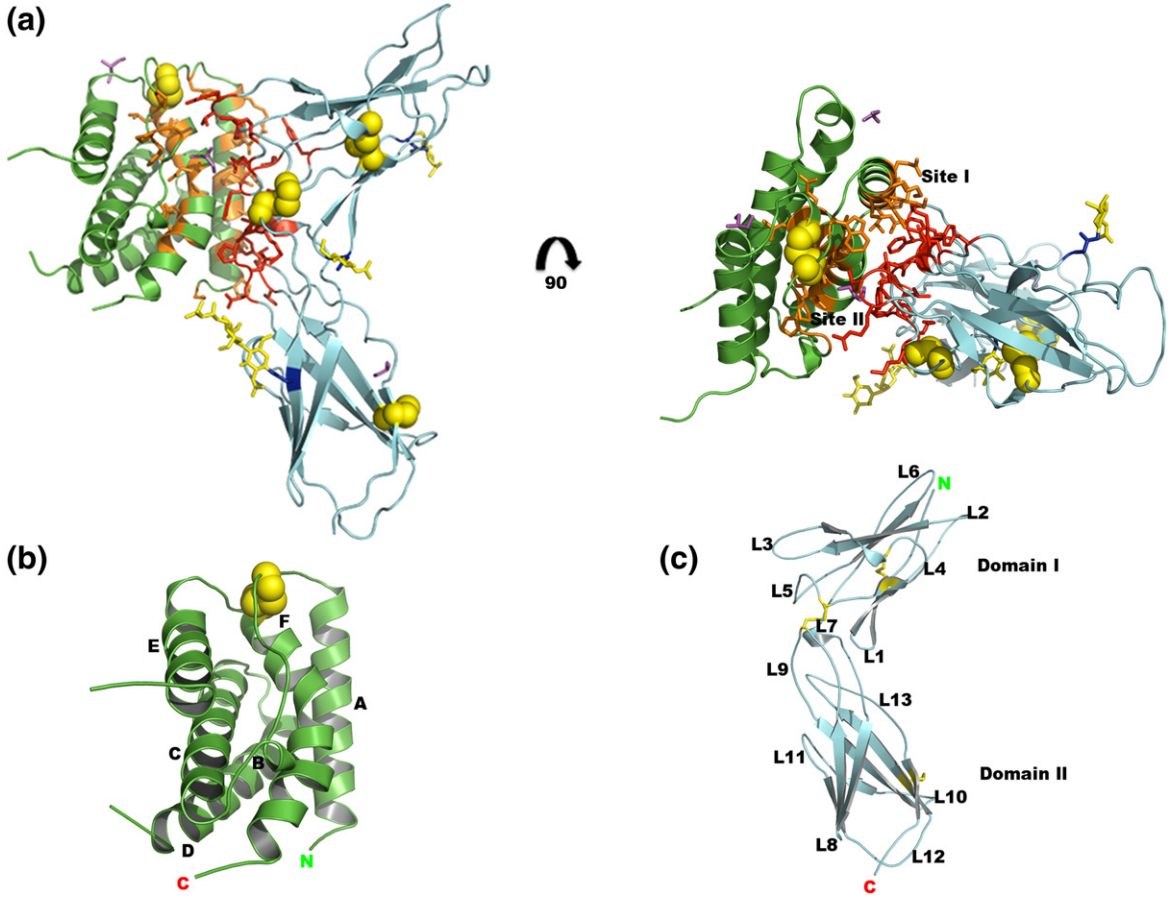

Fig. 1. Structure of the complex of IFN-λ1 and IFN-λR1. (a) IFN-λ1 is in green, IFN-λR1 is in cyan, glycosylation sites are in blue (Asn) and yellow (carbohydrates), glycerol is in magenta, disulfide bonds are yellow spheres, IFN-λ1 residues at the interface are in orange, and IFN-λR1 residues at the interface are in red. Amino acid side chains, carbohydrates, and solvent molecules are depicted in stick format. The location of the site 1 and site 2 interfaces is labeled. (b) The structure of IFN-λ1, in the same orientation as is found in (a). The helices found in the ligand are labeled A through F with the N and C termini also labeled. (c) The structure of IFN-λR1, in the same orientation as found in (a). The loops found in the receptor are labeled, from L1 to L13. The N and C termini are labeled as well. Disulfide bonds are depicted as yellow sticks.

be discussed below. The parts of the IFN-λ1$_{ins}$/IFN-λR1 complex that could be modeled contain residues 22–170 of IFN-λ1 and residues 4–203 of IFN-λR1. In addition, 268 water molecules, 3 glycerol molecules, and N-linked glycosylation sites at Asn9, Asn16, and Asn122 of IFN-λR1 were also modeled. The model possesses good stereochemistry as evaluated by MolProbity, with no residues found in disallowed regions of the Ramachandran plot. IFN-λ1$_{ins}$/IFN-λR1 was refined to final *R*-factors of 0.1836 and 0.2278 for R_{work} and R_{free}, respectively.

Structure of IFN-λ1 bound to IFN-λR1

A molecule of IFN-λ1 is composed of six helices (A–F; Fig. 1), with helices A, C, D, and F forming a classical up–up–down–down four-helix bundle.[48] Topologically, IFN-λ1 is similar to IL-10 and to other members of the IL-10 family, particularly IL-19[37] and IL-22.[29,38] A unique feature of the structure of IFN-λ1 compared to the cytokines mentioned above is the absence of the short helix A′ (which was not visualized in the electron density) preceding the main body of helix A. A similar feature has been found in the structure of IFN-λ3,[29] whose amino acid sequence is 84% identical with IFN-λ1, in spite of the fact that most of the differences were found at the N termini of the proteins, amino residues 1–13 (Fig. 2). (Unless mentioned otherwise, IFN-λ1 numbering has been used throughout this article.)

IFN-λ1 differs from the other two members of the type III IFN family by its pattern of disulfide bridges. Only five cysteines are present in IFN-λ1, while IFN-λ2 and IFN-λ3 possess seven cysteines. The disulfides are formed in IFN-λ1 between Cys49-Cys145 and Cys112-Cys171, whereas the disordered Cys15 is free. In IFN-λ3, disulfide bridges are formed between Cys16 and Cys115, between Cys50 and Cys148, and between Cys167 and Cys174, whereas Cys48 is free in solution but makes an intermolecular disulfide bridge with Cys48 of a neighbor molecule in the crystal (IFN-λ3 numbering).[29]

Although the IFN-λ1 used to make the IFN-λ1$_{ins}$/IFN-λR1 crystals was produced in *Drosophila* S2 cells where N-linked glycosylation occurs, no evidence for its glycosylation at Asn46 was found in the electron density. This observation, however, is not a proof of the lack of glycosylation but most likely the result of the influence of the crystal-packing contacts between loop AB of IFN-λ1 and helix D of a symmetrically related molecule that prevent the putative glycosylation at Asn46 from being visualized in the electron density.

While the crystallographic symmetry results in the creation of dimers of IFN-λ1, such dimers do not bear any similarity to the true dimers seen in the structure of IL-10.[35] This is likely due to the lattice packing of the IFN-λ1$_{ins}$/IFN-λR1 and IFN-λ1$_{bac}$/IFN-λR1 complexes as compared to the restraints imposed on the free IFN-λ1 or IL-10 in their respective crystal-packing environments. Consequently, the IFN-λ1/IFN-λR1 complex forms in a 1:1 ratio as opposed to the 1:2 ratio of dimeric IL-10 to IL-10R1 found in IL-10/IL-10R1 complexes.[16,35,36]

Structure of IFN-λR1

The structures presented here are the first for IFN-λR1 and, as such, give insights into ligand recognition and binding. A molecule corresponding to the extracellular portion of IFN-λR1 is composed of two β-sandwich domains D1 and D2 (Fig. 1), with each domain formed by a sandwich of two β sheets (with each sheet composed of three or four stands). The domains are linked by a loop with a short helical turn in the middle of L7. An equivalent conformation was also found in other hematopoietic cytokine receptors and was labeled fibronectin type III domains.[50] The fibronectin type III domains are oriented with a domain angle of 112° to one another, with the ligand binding to the receptor at the apex between the two domains. The inter-domain angles were measured using C^{α} carbon positions of Glu104, Pro30, and His173 of IFN-λR1, which are equivalent to residues used to define the inter-domain angle of IL-22R1.[39] The inter-domain angle is smaller than that reported for IL-22R1 but very

Fig. 2. Alignment of the IFNs and their receptors. (a) Depiction of the alignment of IFN-λ1, IFN-λ2 and IFN-λ3 to one another. Exclamation points below the sequence indicate the location of sites where mutation of IFN-λ3 has been shown to impact activity. Identical amino acid residues are shown in green, glycosylation sites are in pink, signal peptide is in purple, variations are in red, and cysteines are in yellow; purple indicates residues not visualized to date in any known structure. Blue lettering above the sequences indicates the location and type of the secondary-structure element found in IFN-λ or IFN-λR1, with b indicating a β strand and h indicating the presence of a helix. "∗" indicates a conserved residue, ":" indicates a partially conserved residue, and "." indicates the presence of similar residues. Disulfide bridges in IFN-λ1_Human: Cys15 is free, Cys49-Cys145, Cys112–171. Disulfide bridges in IFN-λ3_Human: Cys16-Cys115, Cys50 is free, Cys50–148, Cys167–174.[29] Swiss-Prot[49] accession numbers are Q8IU54 for IFN-λ1_Human, Q8IZJ0 for IFN-λ2_Human, and Q8IZI9 for IFN-λ3_Human. (b) Alignment of the ectodomain of IFN-λR1 to the equivalent domains in IL-10R1, IL-10R2, and IL-22R1. Magenta lettering in this alignment indicates regions that have not been visualized in the available crystal structures. Cysteines are highlighted in yellow. Symbols below the alignment are identical with those in (a).

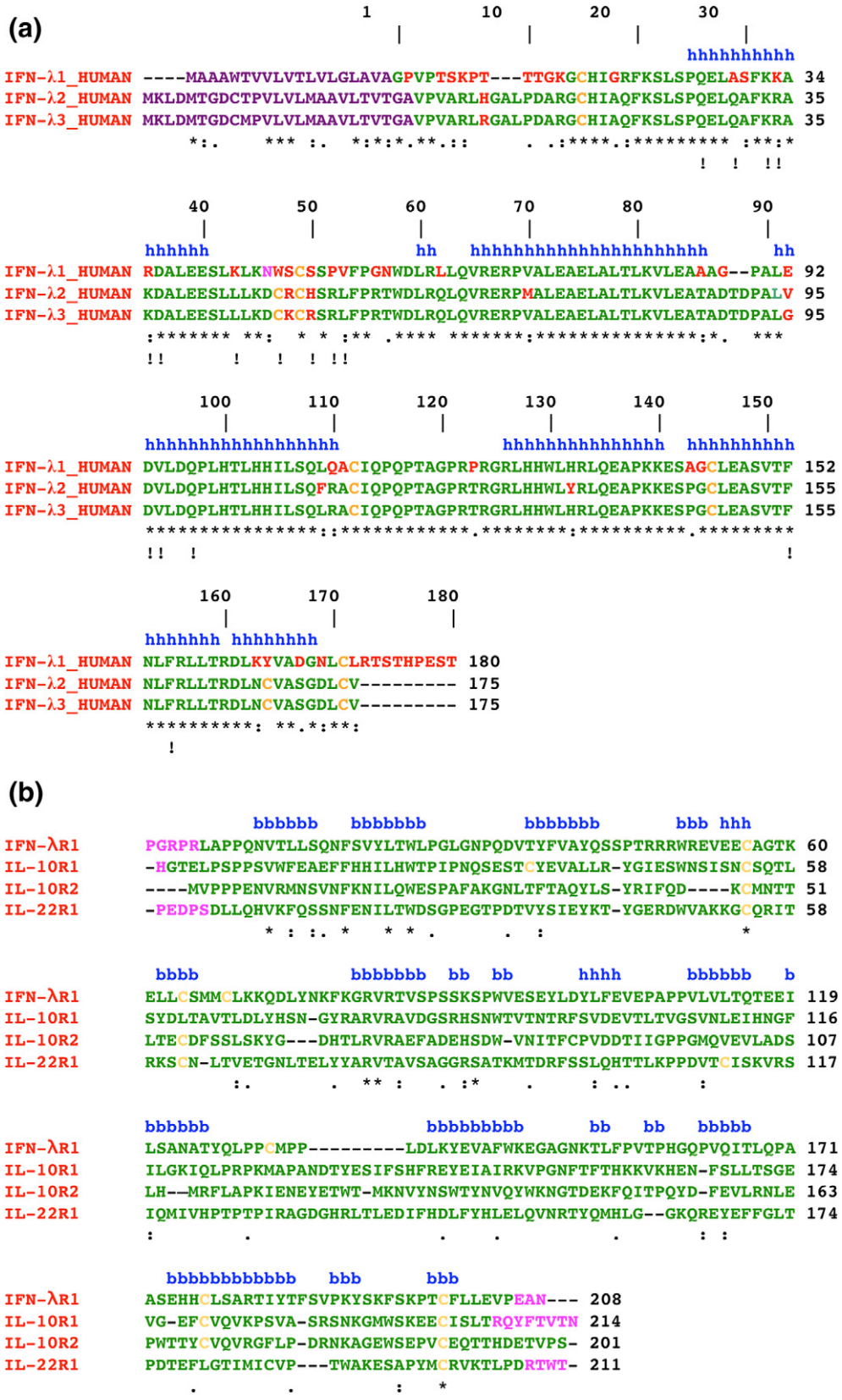

Fig. 2 (*legend on previous page*)

similar to the value reported at equivalent positions in IL-10R1.[39] Of the 13 loops joining β-strands, 5 (L3, L5, L7, L9, and L13) participate in the interactions with ligand and are labeled in Fig. 1. The contacts between IFN-λR1 and IFN-λ1 are primarily hydrophobic in nature (see below).

An important feature unique to IFN-λR1 and not present in most other cytokine receptors is an inter-domain disulfide bridge between Cys66 and Cys130. This disulfide is not found in other cytokine receptors with known structure, with IFN-γ being the only exception so far.[51] This disulfide bridge links D1 and D2 together and limits possible inter-domain movements. Such restriction certainly affects the binding specificity of the receptor toward its ligand; however, the inter-domain orientation is highly similar to IL-10R1 and IL-10R2. It is likely that the inter-domain restrictions imposed by the Cys66-Cys130 disulfide impede conformational changes during formation of the ternary IFN-λ/IFN-λR1/IL-10R2 complex and contribute to preventing other IFNs and ILs from signaling through the IFN-λR1/IL-10R2 receptor complex, presumably maintaining receptor–ligand specificity.

Glycosylation sites are present at the side chains of Asn9, Asn16, and Asn122 of the receptor. Asn9 and Asn16 are linked to a single visible *N*-acetylglucosamine (NAG) moiety, while Asn122 is modified with NAG–NAG–mannose. In the structure of IFN-$\lambda 1_{bac}$/IFN-λR1, the carbohydrate at Asn122 forms contacts with a symmetrically related molecule of IFN-λR1 to help build the crystal lattice (Supplemental Fig. S1). Based on the details of the ternary complexes of IL-10R2 with CMV IL-10 and IL-10R1,[28] it would appear that the glycosylation sites are not in a position to interfere with the formation of the ternary complex.

Structure of the complex

The IFN-λ1/IFN-λR1 complex is composed of one molecule of IFN-λ1 bound to one molecule of IFN-λR1. Unlike the structure of CMV IL-10 in complex with IL-10R1, there is no evidence of disulfide-linked dimer formation.[36] Binding occurs between two complementary surfaces made by helix A, loop AB, and helix F on the side of the ligand, whereas the surface of the receptor in the vicinity of the inter-domain area includes loops L3, L5, and L7 of domain D1 and loops L9 and L13 of domain D2 (Fig. 3). None of the oligosaccharides are involved in the ligand–receptor interactions. The amino acid residues involved in the interface on the surface of IFN-λ1 are Pro25, Leu28, Lys32, Arg35, Asp36, Glu39, Trp47, Phe54, Phe152, Phe155, Arg156, and Arg160 (Fig. 3), whereas the amino acid residues on the side of the IFN-λR1 are Pro43, Thr44, Tyr73, Asn74, Lys75, Asp98, Leu100, Phe101, Pro133, Asp135, Thr183, Phe184, and Ser185. The interaction surface is tightly packed, is hydrophobic, is largely solvent free, and has a shape complementarity (Sc) value[52] of 0.644. The Sc value for the IFN-$\lambda 1_{bac}$/IFN-λR1 structure is 0.641. These Sc values are similar to those of antibody–antigen complexes,[52] suggesting a strong association between IFN-λ1 and IFN-λR1.

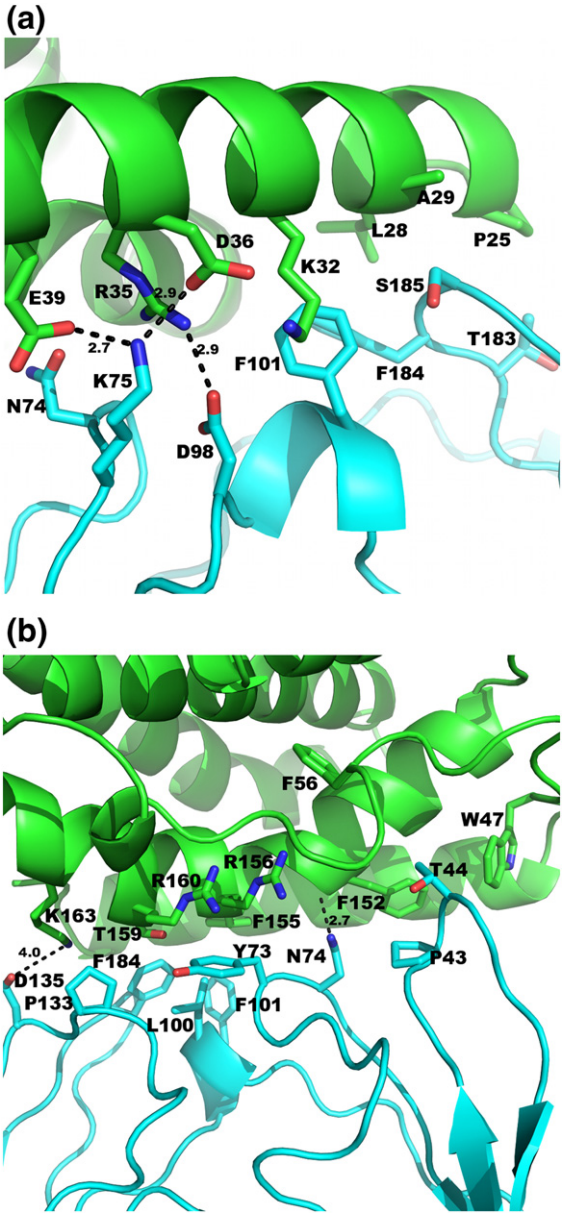

Fig. 3. Interactions between IFN-λ1 and IFN-λR1. IFN-λ1 is depicted in green while IFN-λR1 is depicted in cyan, with residues making contacts depicted in stick format. Oxygens are colored red and nitrogens are colored blue. (a) Site 1 interactions are depicted, with hydrogen bonds formed between the ligand and the receptor depicted as broken lines and their distances listed. (b) Site 2 interactions between the ligand and the receptor are shown, with identical coloring as in (a).

The interactions between IFN-λ1 and IFN-λR1 consist largely of van der Waals and hydrophobic contacts as opposed to hydrogen bonds. For the purposes of this discussion, the interactions have been placed into two groups: interactions between helix A of the ligand with loops L5, L7, and L13 of the receptor (site 1) and interactions between helix F of the ligand with loops L3, L5, L7, L9, and L13 of the receptor (site 2). The interaction between IFN-λ1 and IFN-λR1 buries 703 and 803 $Å^2$ of surface area on IFN-λ1 and IFN-λR1, respectively.

At site 1, helix A contains several residues that make hydrogen bonds to the receptor. Hydrogen bonds are made between Asp36 of the ligand and Lys75 of the receptor (2.9 Å), between Glu39 of the ligand and Lys75 of the receptor (2.7 Å), and between Arg35 of the ligand and Asn74 and Asp98 of the receptor (2.9 and 3.8 Å, respectively) (Fig. 3). As mentioned before, the interface between the ligand and the receptor is largely solvent free; however, two waters do bridge hydrogen bonds (between Arg35 of the ligand and Asp98 of the receptor and between Glu39 of the ligand and Arg46 of the receptor). The relative paucity of direct bonds as compared to nonbonded contacts (4 hydrogen bonds *versus* 36 nonbonded contacts) further suggests that hydrogen bonds are only responsible for initial recognition of the ligand by the receptor, while the more numerous hydrophobic contacts solidify the interaction.

Site 2 is similar to site 1 in that relatively few hydrogen bonds are formed between the ligand and the receptor (Fig. 3). At helix F, a hydrogen bond is only made between the main-chain carbonyl of Phe152 (ligand) and Asn74 of the receptor (2.7 Å). A salt bridge is found between Asp135 of the ligand and Lys163 of the receptor. Again, the few direct bonds that are present likely contribute to initial recognition of the ligand, while the large number of nonbonded hydrophobic contacts at helix F (30) solidifies the interaction between ligand and receptor.

Comparison to other structures

IFN-λR1 is highly similar to other IL receptors, in particular IL-10R1 and IL-10R2. All of these receptors share a common two-domain fold consisting of two repeats of a fibronectin type III domain, with a linking loop in between. Structural differences exist, most notably that IL10R1 contains an α helix where Loop 5 is found at the inter-domain interface of IFN-λR1. This short α helix is also not found in IL-10R2.

The main differences between IL-10R2 and IL-λR1 are the presence of an α helix at the C terminus of IL-10R2, a small β sheet followed by a short α helix in between the fibronectin domains of IL-10R2 (located where Loop 8 is found in IFN-λR1), and the presence of another short α helix in IL-10R2 where a loop is found in IFN-λR1. The α helix and β sheet found in the inter-domain region of IL-10R2 may contribute to the lower affinity of that receptor for IFN-λ1.

IFN-λR1 has a C^{α} root-mean-square displacement (rmsd) of 3.0 Å when aligned to IL-10R1, 2.9 Å when aligned to IL-10R2, 2.6 Å when aligned to IL-22R1, and 2.0 Å when aligned to IL-22BP. Also, when compared to IL-10R2, several clefts that are not found in IFN-λR1 are evident in IL-10R2 (Fig. 4), specifically clefts 2/3 and 3/5 as described by Yoon *et al.*[28] In this way, IFN-λR1 is much more similar to IL-10R1 and IL-22BP in structure, further supporting the notion that IL-10R2 possesses unique adaptations to allow for binding to a number of cytokines and receptors.

While the interaction of IL-22 with its full receptor complex has been modeled,[28] the sequence conservation at the key interaction site between IL-22 and IL-10R2 is not high when compared to IFN-λ1. Specifically, the model indicates that interactions occur between IL-22 residues Glu101, Phe105, Asp109, and Gln116 with residues Tyr56, Tyr59, Arg10, and Gln63 from IL-10R2. Few residues corresponding to the IL-22 residues are found in IFN-λ1 when a structural alignment is made, making modeling of a full IFN-λ1/IFN-λR1/IL-10R2 complex difficult. This also suggests that IFN-λ1 may engage both components of the full receptor complex primarily through association with the high-affinity IFN-λR1 and that interactions with IL-10R2 may be bridged through interactions between IFN-λR1 and IL-10R2.

IFN-λ1 also shows a high level of similarity to other IFNs and ILs. All of these signaling molecules share a similar helical bundle fold, although they differ in some detail, as well as in their oligomeric state. Not surprisingly, when their backbones are aligned based on C^{α} coordinates, IFN-λ1 is found to be most similar to IFN-λ3, with an rmsd of 1.0 Å. IFN-λ1 is also structurally similar to other IFNs and ILs with known structure identified as members of the IL-10 family, with a 3-Å rmsd to IL-22 [Protein Data Bank (PDB) code 1M4R],[38] a 3.2-Å rmsd to IL-10 (PDB code 1LK3),[53] a 3.2-Å rmsd to IL-19 (PDB code 1N1F),[37] a 3.2-Å rmsd to IFN-γ (PDB code 1EKU),[54] and a 3.2-Å rmsd to IFN-β (PDB code 1AU1).[55]

Discussion

Two crystal structures of IFN-λ1, a type III IFN, were determined in complex with the extracellular domain of its receptor IFN-λR1. Differences in crystal packing did not significantly influence the structures of the complexes. The structure of IFN-λ1 itself is highly similar to the structure of IFN-λ3, as well as IL-22 and IL-10. IFN-λR1 contains two domains consisting of fibronectin type III repeats, similarly to IL-10R1 and IL-22R1. The complex

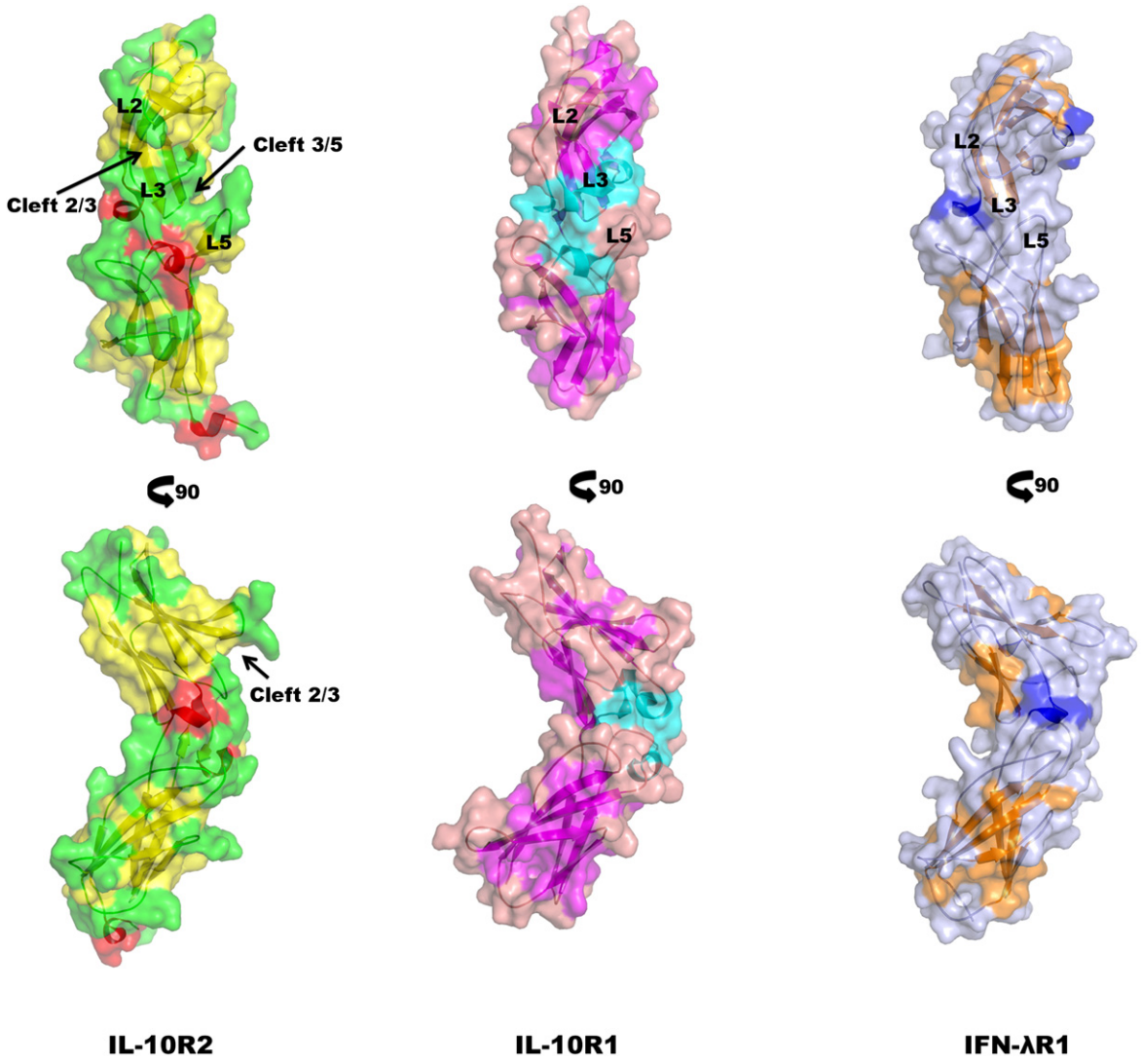

Fig. 4. IFN-λR1 is more structurally homologous to IL-10R1 than to IL-10R2. Surface comparison is based on the data of Yoon *et al.*[28] Clefts identified as being important for receptor promiscuity in IL-10R2 (labeled in IL-10R2) are not found in IFN-λR1 or IL-10R1. The identities of the models are shown below.

between IFN-λ1 and IFN-λR1 is defined primarily by helices A and F on IFN-λ1 and several loops on IFN-λR1 and is primarily hydrophobic in nature. Several hydrogen bonds and salt bridges are found between the two proteins, but these are far fewer than the interaction surface provided by nonbonded interactions through hydrophobic amino acids at the interface surface. The structure suggests that binding of IFN-λ1 by IFN-λR1 is initiated by amino acids capable of making complementary electrostatic interactions and solidified by hydrophobic interactions between the ligand and receptor.

Comparisons with other IFNs and ILs

Structural alignment of IFN-λ1/IFN-λR1 to cytokines or receptors found in other ligand–receptor complexes immediately demonstrates that IFN-λ1 binds to IFN-λR1 in a manner distinct from other complexes such as IL-10 bound to IL-10R1. Similarly to the interactions seen in the IL-10/IL-10R1 complex, significant nonpolar and a few electrostatic contacts are made between IFN-λ1 and IFN-λR1 through helices A and F of the ligand to inter-domain loops of the receptor. However, when IFN-λR1 is aligned to IL-10R1, the ligands are bound to different portions of their respective receptors. IFN-λ1 binds such that it is roughly perpendicular to the hinge region between the fibronectin domains of IFN-λR1, whereas IL-10 binds to IL-10R1 at the inter-domain regions but rotated ~35° out of a plane formed through the fibronectin domains (Fig. 5). Similar results are seen when alignment

of IFN-λ1/IFN-λR1 to other ligand–receptor complexes is performed (not shown).

The unique binding orientation utilized by IFN-λ1 could be explained in several ways. First and most likely is that the binding mode has evolved between IFN-λ and its receptor to ensure recognition of IFN-λ only upon presentation of various cytokines at the cell surface. Second, the binding of IL-10 to its receptor may be influenced by the formation of dimers of IL-10. Given that the dimer of IL-10 is thought to be the functional form of the cytokine, the interaction with IL-10R1 may require a slightly different surface to accommodate IL-10. Finally, the differences in ligand–receptor orientation could be influenced by lattice-packing requirements that alter the interaction between IFN-λ1 and IFN-λR1. However, the observation that mutations of IFN-λ3 that greatly disrupt its activity are located directly at the ligand–receptor interface argues against this point.

Activity of IFN-λ members and receptor binding

It has been established that the antiviral activity of the three known members of the IFN-λ family is such that IFN-λ3>IFN-λ1>IFN-λ2,[24] with IFN-λ3 being 16-fold more active than IFN-λ2, despite only seven amino acid variations between λ3 and λ2 (Fig. 2). Of these variations, one is not visualized in any IFN-λ structure (H/R variance at position 28, numbered from the beginning of the signal peptide). Interestingly, when the variant positions are mapped to the IFN-λ1/IFN-λR1 complex, none of the variations occur at the interface and are localized to helices C, D, and E, as well as loop AB (Supplemental Fig. S2).

While the variations may be subtly influencing the positioning of helices A and F to change the interactions with IFN-λR1, it is more plausible that the variations are influencing the binding of IFN-λ1 by the receptor partner IL-10R2. Unfortunately, the details of the interface between any cytokine with IL-10R2 have yet to be determined, although several models have been proposed for the complex formation.[28,34] In the models of the IL-22/IL-22R1/IL-10R2 complex, interactions occur between helix D of the ligand with loops L2 and L3 of the receptor, along with interactions between helix A and L5.

Of the specific variations, two occur on helix D where the interaction with IL-10R2 has been modeled in the IL-22/IL-22R1/IL-10R2 complex. These variations (Val95Gly and Phe112Leu in λ2 and λ3, respectively) are not likely to alter the electrostatic interactions between IFN-λ and IL-10R2 but may impact the positioning of helix D or slightly disrupt the hydrophobic surface for binding of IL-10R2. It is likely that the variations found between IFN-λ3 and IFN-λ2 affect the interaction with IL-10R2 and thereby may result in altered signaling intensity or duration, leading to the differential expression of antiviral genes.

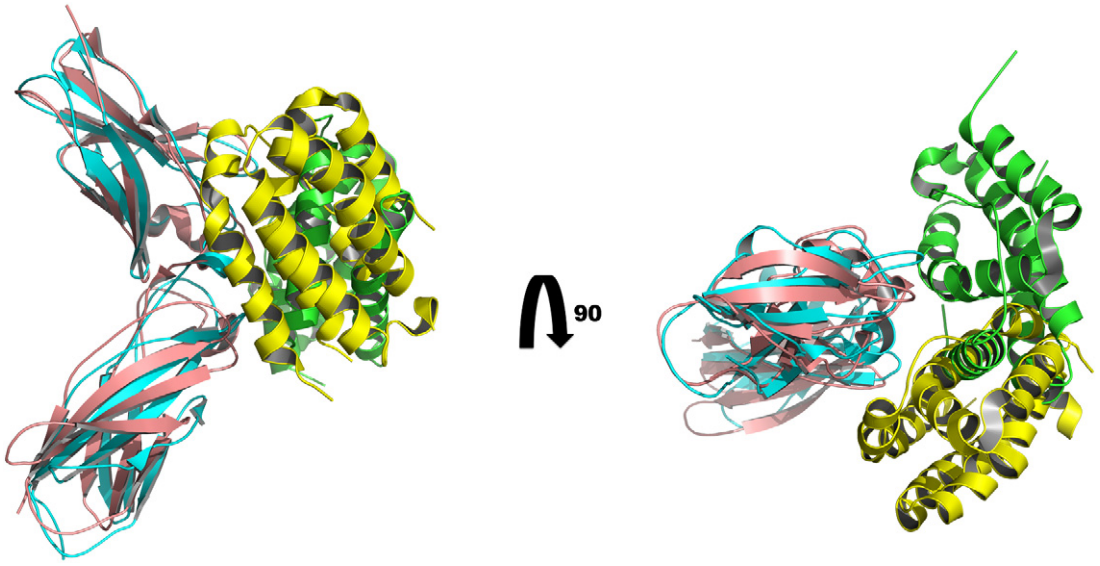

Fig. 5. IFN-λ1 and IL-10 bind to different sites on their respective high-affinity receptors. An alignment of IFN-λR1 to IL-10R1 was performed, and the positions of their respective ligands, IFN-λ1 and IL-10, were added. IL-10 is a composite containing helices A through D of one monomer of IL-10 and helices E and F of the dimeric partner. The IFN-λ1/IFN-λR1 complex is displayed in green/cyan and the IL-10/IL-10R1 complex is displayed in yellow/rose. For IL-10/IL10-R1, only one-half of the IL-10 dimer is displayed.

Interpreting the influence of mutagenesis on IFN-λ3 activity

It has been reported that mutations of IFN-λ3 can strongly impact its antiviral activity, and many of the sites of mutation were presumed to make contacts with the receptor.[29] In IFN-λ3, mutagenesis at Gln30, Cys48, Arg51, and Asp96 revealed weak disruption of its activity (<5-fold increase in EC_{50}). A stronger impact on activity (5- to 25-fold increase in EC_{50}) was found by mutating Gln27, Leu44, Arg53, and Leu54, whereas a very strong impact on activity (>25-fold increase in EC_{50}) was found at Lys33, Arg34, Lys36, Asp37, Val97, Gln100, Phe155, and Phe158.

The corresponding residues in IFN-λ1 are as follows (IFN-λ1 numbering used): weak impact equivalents at Gln29, Trp47, Ser50, and Asp93; strong impact equivalents at Gln26, Lys43, Pro52, and Val53; and very strong impact equivalents at Lys32, Lys33, Arg35, Asp36, Val94, Gln97, Phe152, and Phe155. Mutations of Phe152 and Phe155, which strongly impacted the activity of IFN-λ3, are positioned at critical points at the IFN-λ1/IFN-λR1 interface where these residues make nonbonded contacts to Pro43, Thr44, Asn74, Leu100, Phe101, and Phe184 of the receptor. While mutation to alanine would preserve the nonpolar nature of the amino acid, large changes to the hydrophobic surface in IFN-λ3 occur, likely preventing efficient binding to IFN-λR1. The Phe158Ala mutation almost completely eliminated the activity of IFN-λ3, and based on the structure of the IFN-λ1/IFN-λR1 complex presented here, it is highly likely that a corresponding Phe155Ala mutation would completely disrupt the interactions of IFN-λ1 with IFN-λR1. With the exception of the Phe158Ala mutation that was almost completely inactive, the ability of the other IFN-λ3 mutants to still inhibit encephalomyocarditis virus infection is likely due to the compensatory nature of the hydrophobic interface.

A similar situation exists around Lys32, Arg35, and Asp36 in IFN-λ1. Lys32 makes nonpolar contacts with Phe101 of the receptor, Arg35 makes hydrogen bonds to Asp96 of the receptor as well as other nonbonded interactions, and Asp36 makes a hydrogen bond with Lys75 of the receptor. The mutation of the corresponding residues in IFN-λ3 greatly decreased its antiviral activity, in this case likely due to disruption of both electrostatic and nonpolar interactions between IFN-λ3 and IFN-λR1.

The equivalents of several residues shown to affect the activity of IFN-λ3, including Gln26, Lys33, Lys43, Ser50, Trp47, Pro52, Val53, and Asp93, do not appear at the interface between IFN-λ1 and IFN-λR1. It is likely that mutations at each of these positions impact the positioning of helices A and F for binding of IFN-λ to IFN-λR1 or that the mutations disrupt proper folding of IFN-λ3. Val94 and Gln97 also do not directly contact IFN-λR1; however, they are positioned immediately adjacent to helix A on the surface of IFN-λ molecules and likely disrupt the proper positioning of helix A in the mutations made to IFN-λ3. Another possibility is that while folding is maintained and the interaction with IFN-λR1 is not impacted, the binding of IFN-λ3 to IL-10R2 is inhibited, thus preventing proper signaling by IFN-λ.

IFN-λ1 interactions with Yaba-like disease virus

It has been recently reported that a glycoprotein secreted by the Yaba-like disease virus can competitively bind to and simultaneously inhibit the activity of type I and type III IFNs.[56] This protein, Y136, shows low sequence homology to another IFN antagonist, B18, produced by the vaccinia virus. Knowledge of the interaction of these secreted glycoproteins with the IFNs may provide clues to the development of more effective antiviral drugs to treat diseases caused by the members of the *Poxviridae* family.

Ternary complex modeling

Using the models of ternary complexes of two members of the IL-10 family provided by Mark Walter[28] (IL-22/IL-22R1/IL-10R2 or cmvIL-10/IL-10R1/IL-10R2), it is possible to gain some insight into the type of interactions expected in the ternary complex of IFN-λ and its receptors. When an alignment of the IFN-λ1/IFN-λR1 complex to IL-10R1 or IL-22R1 is made using only IFN-λR1, the resulting position of IFN-λ1 is drastically different from the modeled positions of cmvIL-10 or IL-22. As a result, IFN-λ1 makes no contacts with IL-10R2 in its modeled position as part of the heterodimeric receptor complex. However, when the alignment of the IFN-λ1/IFN-λR1 complex is made by matching IFN-λ1 to cmvIL-10 or IL-22, IL-10R2 is positioned to make contacts with IFN-λ1 (Supplemental Fig. S3a and S3b).

Furthermore, when the IFN-λ3 mutations that are known to affect its activity[29] are mapped to the ternary IFN-λ1/IFN-λR1/IL-10R2 model, a number of residues (Gln26, Lys33, Asp93, Val94, Phe152, and Phe155) equivalent to those strongly impacting the activity of IFN-λ3 are localized near the potential IFN-λ/IL-10R2 interface (Supplemental Fig. S3c). This suggests that the IFN-λ3 mutations may have impacted anti-encephalomyocarditis virus activity via disruption of the interaction with IL-10R2.

When visualizing the IFN-λ2/3 variations in the context of the ternary complex, the interpretation of the variations is less clear. None of the variations occur at the interface between IFN-λ1 and IL-10R2,

Table 1. X-ray data collection and refinement statistics

	IFN-λ1$_{bac}$/ IFN-λ1R1	IFN-λ1$_{ins}$/ IFN-λ1R1
Data statistics		
Space group	$P2_12_12$	$P2_12_12_1$
Unit-cell parameters (Å)	a=130.2, b=65.4, c=73.2	a=65.0, b=85.8, c=116.5
Resolution (Å)	2.16	2.1
Measured reflections	122,399	258,890
Unique reflections	33,364	37,819
Completeness (%)[a]	97.4 (81.7)	97.1 (79.6)
Redundancy[a]	3.7 (2.7)	6.8 (4.2)
R_{merge}[a,b]	0.057 (0.71)	0.07 (0.84)
$I/\sigma(I)$[a]	16.8 (1.9)	23.6 (2.2)
Refinement statistics		
Resolution[a]	29.1–2.16 (2.28–2.16)	29.4–2.1 (2.19–2.1)
R_{work}[c]	0.198	0.184
No. of reflections (R_{work})	30,089	34,990
R_{free}[d]	0.2402	0.2278
No. of reflections (R_{free})	926	1054
No. of residues		
IFN-λ1	140	143
IFN-λ1R1	197	200
No. of waters	148	268
No. of glycerols	0	3
No. of carbohydrates	4	5
rmsd bond distance (Å)	0.005	0.01
rmsd bond angles (°)	1.05	1.22
B-factors		
Average (all atoms)	71.2	67.8
Protein atoms	71.4	68.1
Solvent	68.1	61.1
Ramachandran plot (%)		
Favored	96.7	95
Allowed	3	5
Disallowed	0.3	0

[a] Data in parentheses refer to the highest-resolution shell.

[b] $R_{merge}=(\sum|(I(i)-\langle I(h)\rangle|)/(\sum I(i))$, where $I(i)$ is the ith observation of the intensity of a reflection with indices (h,k,l) and $\langle I(h)\rangle$ is the average intensity of all symmetry equivalent measurements of that reflection.

[c] $R_{work}=\sum|F_o(h)-F_c(h)|/\sum|F_o(h)|$, where $F_o(h)$ and $F_c(h)$ are the observed and calculated structure factor amplitudes, respectively.

[d] $R_{free}=\sum|F_o(h)-F_c(h)|/\sum|F_o(h)|$, calculated with the test set data where $F_o(h)$ and $F_c(h)$ are the observed and calculated structure factor amplitudes, respectively.

with most of the residues modeled as exposed to solvent (Supplemental Fig. S3d). This suggests that the IFN-λ2/3 variations do not directly impact binding to either IFN-λR1 or IL-10R2 but rather indirectly impact binding to those receptor components through subtle rearrangements of IFN-λ. These rearrangements of IFN-λ may be enough to produce the 16-fold difference in activity seen between λ2 and λ3.[24] It is of interest to note that independent genome-wide association studies identified several SNPs within the region of the IFN-λ3 gene, which were not only correlated with the spontaneous clearance of HCV[44] but also associated with sustained virologic response in patients with chronic HCV undergoing pegylated IFN-α/ribavirin combination therapy.[42–44,46] These genetic variants within the IFN-λ3 gene locus are likely to affect the level of expression and/or biological activity of IFN-λ3. Interestingly, one of these SNPs causes substitution of Lys48 to Arg, representing the natural IFN-λ2/3 variation. It remains to be studied whether this substitution affects receptor interaction and biological potency of IFN-λ3.

Summary

We have reported here the first structure of IFN-λ1 in complex with its cellular receptor, IFN-λR1. Both the ligand and the receptor exhibit topology similar to that of other known cytokines and cytokine receptors, respectively, with a number of subtle variations. The structure of the complex suggests that long-range electrostatic interactions help to orient IFN-λ1 for binding to IFN-λR1, while hydrophobic and nonpolar interactions solidify the interface between the ligand and the receptor. The structure offers insights into the phenotypes of IFN-λ3 mutations in regard to its antiviral activity and suggests how variances between IFN-λ members influence the differential antiviral activity of these cytokines. However, an experimentally derived structure of the ternary complex that also would include the IL-10R2 receptor molecule is needed for the fuller understanding of the antiviral activity of type III IFNs.

Materials and Methods

Protein production and purification

Protein production and purification were performed as previously described.[47] Human IFN-λ1 (encoding amino acids 1–181) and human IFN-λR1 were cloned into pMT/BiP/V5-His carrying a BiP *Drosophila* signal peptide upstream of an N-terminal His_6 tag. Protein was expressed in *Drosophila* S2 cells and secreted directly into the media. Human IFN-λ1 (encoding amino acids 2–181) expressed in *E. coli* was purchased from Peprotech.

IFN-λ1 and IFN-λR1 were purified using copper affinity chromatography (GE Healthcare Fast Flow Chelating Sepharose) followed by a size-exclusion column (GE Healthcare Superdex-75 HiLoad 16/60). Activity of purified IFN-λ1 was verified by demonstrating its ability to induce signal transducer and activator of transcription activation using electrophoretic mobility shift assay[2] while the activity of IFN-λR1 was assessed by its ability to form complexes with IFN-λ1.

Complexes of IFN-λ1 and IFN-λR1 were generated by mixing equimolar amounts of IFN-λ1 (from *E. coli* or *Drosophila* cells, here called IFN-λ1_{bac} and IFN-λ1_{ins}, respectively) with IFN-λR1 and incubating at room temperature for 120 min. The complexes were centrifuged and subsequently purified on a gel-filtration column. Approximately 3-mg yields were achieved during purification. Final samples were pooled and concentrated to ~6 mg/ml for crystallization.

Crystallization

Crystallization screening experiments were executed in sitting drops using a Phoenix crystallization robot (Art Robbins Instruments). Crystallization screens utilized for preliminary experiments were Index (Hampton Research), polyethylene glycol (PEG), and pHClear (Nextal Biotechnologies). Crystals were optimized in EasyXtalTools 24-well plates (Qiagen) using 0.75 ml well volumes and drops consisting of 2 μl protein and 1 μl precipitant. For the IFN-λ1_{bac}/IFN-λR1 complex, crystals were grown in 17% PEG 3350 and 100 mM Hepes, pH 7.8, while for the IFN-λ1_{ins}/IFN-λR1 complex, crystals were grown in 20% MPEG 2000, 100 mM Tris–HCl, pH 7.9, and 200 mM trimethylamine *N*-oxide dehydrate. Crystals of both complexes appeared within 1 day and reached their maximal size in 4 days.

Data collection, integration, and phasing

Data collection and processing were performed as previously described.[47] Briefly, diffraction data were collected at beamline 22-ID at the Advanced Photon Source, Argonne National Laboratory. Crystals were cryoprotected in solutions composed of well solution supplemented with glycerol to a final concentration of 20% v/v and then frozen directly in a nitrogen stream at 100 K. Diffraction data extended to 2.1 and 2.16 Å resolution for the IFN-λ1_{ins}/IFN-λR1 and IFN-λ1_{bac}/IFN-λR1 crystals, respectively. Both complexes crystallized in orthorhombic space groups, with IFN-λ1_{ins}/IFN-λR1 crystals forming in space group $P2_12_12_1$, whereas IFN-λ1_{bac}/IFN-λR1 crystals formed in space group $P2_12_12$. Data were merged, scaled, and integrated using DENZO/SCALEPACK,[57] with the statistics listed in Table 1.

Phasing was accomplished through molecular replacement trials utilizing the structures of IFN-λ3 (PDB code 3HHC)[29] and IL-22 binding protein (IL-22BP) (PDB code 3G9V)[41] as search models. Using the program PHASER,[58] we located one copy each of the receptor and the ligand within the asymmetric unit. In what follows, numbering of IFN-λ1 residues in the model is based on the predicted extent of the signal peptide, with the first amino acid occurring after the signal peptide designated as 1. For IFN-λR1, no special numbering scheme was utilized.

Model building and refinement

The receptor complex models were refined against their respective data using PHENIX,[59] with the final refinement and geometry statistics listed in Table 1. The refinement protocol utilized xyz, individual atomic displacement parameter, occupancy (for a single residue with two conformations in INF-λ1_{ins}/IFN-λR1), solvent filtering, and translation/libration/screw refinement, followed by manual model inspection and manipulation in Coot.[60] In the case of the IFN$_{bac}$-λ1/IFN-λR1 complex, occupancy refinement was not utilized. N-linked glycosylation sites were found in both models of the receptor chain, but not in the ligand, despite the fact that in the IFN-λ1_{ins} is glycosylated. Three glycosylation sites were readily identified from $2F_o - F_c$ and $F_o - F_c$ electron density maps (contoured at 1 σ and 3 σ, respectively) in the IFN-λ1_{ins}/IFN-λR1 crystals, whereas only two receptor glycosylation sites were found in the IFN-λ1_{bac}/IFN-λR1 crystals. Model quality was assessed using MolProbity[61] following each cycle of refinement and rebuilding. The refined structures have been deposited in the PDB[62] with the accession codes 3OG6 and 3OG4 for the IFN-λ1_{ins}/IFN-λR1 complex and the IFN-λ1_{bac}/IFN-λR1 complexes, respectively.

Structure analysis

The structures resulting from the work described here, as well as those taken from the literature, were analyzed with a variety of programs. The interfaces between IL-λ1 and IL-λR1 were studied using PISA[63] and PDBSum.[64] DALI[65] was used to compare the structure of the complex to other known structures. Manual inspection of the structures was accomplished using Coot and PyMOL.[66] All structure figures were prepared using PyMOL.

Accession numbers

Coordinates and structure factors have been deposited in the PDB with accession numbers 3OG6 and 3OG4.

Acknowledgements

We would like to thank Dr. Mark Walter for providing us with the coordinates of the models of ternary complexes of cytokines. Diffraction data were collected at Southeast Regional Collaborative Access Team 22-ID (or 22-BM) beamline at the Advanced Photon Source, Argonne National Laboratory. Use of the Advanced Photon Source was supported by the U.S. Department of Energy, Office of Science, Office of Basic Energy Sciences, under Contract No. W-21-109-Eng-38. This project was supported in part by the Intramural Research Program of the National Institutes of Health, National Cancer Institute, Center for Cancer Research, with Federal funds from the National Cancer Institute, National Institutes of Health, under Contract No. HHSN261200800001E, and by the U.S. Public Health Services Grant RO1 AI057468 (S.V.K.) from the National Institute of Allergy and Infectious Diseases. The content of this

publication does not necessarily reflect the views or policies of the Department of Health and Human Services; neither does the mention of trade names, commercial products, or organizations imply endorsement by the U.S. Government.

Supplementary Data

Supplementary data associated with this article can be found, in the online version, at doi:10.1016/j.jmb.2010.09.068

References

1. Kotenko, S. V. & Langer, J. A. (2004). Full house: 12 receptors for 27 cytokines. *Int. Immunopharmacol.* **4**, 593–608.
2. Kotenko, S. V., Gallagher, G., Baurin, V. V., Lewis-Antes, A., Shen, M., Shah, N. K. *et al.* (2003). IFN-λs mediate antiviral protection through a distinct class II cytokine receptor complex. *Nat. Immunol.* **4**, 69–77.
3. Sheppard, P., Kindsvogel, W., Xu, W., Henderson, K., Schlutsmeyer, S., Whitmore, T. E. *et al.* (2003). IL-28, IL-29 and their class II cytokine receptor IL-28R. *Nat. Immunol.* **4**, 63–68.
4. Meager, A., Visvalingam, K., Dilger, P., Bryan, D. & Wadhwa, M. (2005). Biological activity of interleukins-28 and -29: comparison with type I interferons. *Cytokine*, **31**, 109–118.
5. Robek, M. D., Boyd, B. S. & Chisari, F. V. (2005). Lambda interferon inhibits hepatitis B and C virus replication. *J. Virol.* **79**, 3851–3854.
6. Marcello, T., Grakoui, A., Barba-Spaeth, G., Machlin, E. S., Kotenko, S. V., MacDonald, M. R. & Rice, C. M. (2006). Interferons alpha and lambda inhibit hepatitis C virus replication with distinct signal transduction and gene regulation kinetics. *Gastroenterology*, **131**, 1887–1898.
7. Mordstein, M., Neugebauer, E., Ditt, V., Jessen, B., Rieger, T., Falcone, V. *et al.* (2010). Lambda interferon renders epithelial cells of the respiratory and gastrointestinal tracts resistant to viral infections. *J. Virol.* **84**, 5670–5677.
8. Ank, N., West, H., Bartholdy, C., Eriksson, K., Thomsen, A. R. & Paludan, S. R. (2006). Lambda interferon (IFN-lambda), a type III IFN, is induced by viruses and IFNs and displays potent antiviral activity against select virus infections in vivo. *J. Virol.* **80**, 4501–4509.
9. Brand, S., Beigel, F., Olszak, T., Zitzmann, K., Eichhorst, S. T., Otte, J. M. *et al.* (2005). IL-28A and IL-29 mediate antiproliferative and antiviral signals in intestinal epithelial cells and murine CMV infection increases colonic IL-28A expression. *Am. J. Physiol.: Gastrointest. Liver Physiol.* **289**, G960–G968.
10. Doyle, S. E., Schreckhise, H., Khuu-Duong, K., Henderson, K., Rosler, R., Storey, H. *et al.* (2006). Interleukin-29 uses a type 1 interferon-like program to promote antiviral responses in human hepatocytes. *Hepatology*, **44**, 896–906.
11. Zhou, J., Lu, L., Yuen, M. F., Lam, T. W., Chung, C. P., Lam, C. L. *et al.* (2007). Polymorphisms of type I interferon receptor 1 promoter and their effects on chronic hepatitis B virus infection. *J. Hepatol.* **46**, 198–205.
12. Pestka, S., Krause, C. D., Sarkar, D., Walter, M. R., Shi, Y. & Fisher, P. B. (2004). Interleukin-10 and related cytokines and receptors. *Annu. Rev. Immunol.* **22**, 929–979.
13. Lasfar, A., Lewis-Antes, A., Smirnov, S. V., Anantha, S., Abushahba, W., Tian, B. *et al.* (2006). Characterization of the mouse IFN-lambda ligand–receptor system: IFN-lambdas exhibit antitumor activity against B16 melanoma. *Cancer Res.* **66**, 4468–4477.
14. Sommereyns, C. & Michiels, T. (2006). N-glycosylation of murine IFN-beta in a putative receptor-binding region. *J. Interferon Cytokine Res.* **26**, 406–413.
15. Cutrone, E. C. & Langer, J. A. (2001). Identification of critical residues in bovine IFNAR-1 responsible for interferon binding. *J. Biol. Chem.* **276**, 17140–17148.
16. Yoon, S. I., Jones, B. C., Logsdon, N. J. & Walter, M. R. (2005). Same structure, different function crystal structure of the Epstein–Barr virus IL-10 bound to the soluble IL-10R1 chain. *Structure*, **13**, 551–564.
17. Zitzmann, K., Brand, S., Baehs, S., Goke, B., Meinecke, J., Spottl, G. *et al.* (2006). Novel interferon-lambdas induce antiproliferative effects in neuroendocrine tumor cells. *Biochem. Biophys. Res. Commun.* **344**, 1334–1341.
18. Li, Q., Kawamura, K., Ma, G., Iwata, F., Numasaki, M., Suzuki, N. *et al.* (2010). Interferon-lambda induces G1 phase arrest or apoptosis in oesophageal carcinoma cells and produces anti-tumour effects in combination with anti-cancer agents. *Eur. J. Cancer*, **46**, 180–190.
19. Li, W., Lewis-Antes, A., Huang, J., Balan, M. & Kotenko, S. V. (2008). Regulation of apoptosis by type III interferons. *Cell Proliferation*, **41**, 960–979.
20. Guenterberg, K. D., Grignol, V. P., Raig, E. T., Zimmerer, J. M., Chan, A. N., Blaskovits, F. M. *et al.* (2010). Interleukin-29 binds to melanoma cells inducing Jak-STAT signal transduction and apoptosis. *Mol. Cancer Ther.* **9**, 510–520.
21. Numasaki, M., Tagawa, M., Iwata, F., Suzuki, T., Nakamura, A., Okada, M. *et al.* (2007). IL-28 elicits antitumor responses against murine fibrosarcoma. *J. Immunol.* **178**, 5086–5098.
22. Sato, A., Ohtsuki, M., Hata, M., Kobayashi, E. & Murakami, T. (2006). Antitumor activity of IFN-lambda in murine tumor models. *J. Immunol.* **176**, 7686–7694.
23. Abushahba, W., Balan, M., Castaneda, I., Yuan, Y., Reuhl, K., Raveche, E. *et al.* (2010). Antitumor activity of type I and type III interferons in BNL hepatoma model. *Cancer Immunol. Immunother.* **59**, 1059–1071.
24. Dellgren, C., Gad, H. H., Hamming, O. J., Melchjorsen, J. & Hartmann, R. (2009). Human interferon-lambda3 is a potent member of the type III interferon family. *Genes Immun.* **10**, 125–131.
25. Kotenko, S. V. (2007). IFN-λs. In *Class II Cytokines* (Zdanov, A., ed.), pp. 201–211, Transworld Research Network, Kerala, India.

26. Langer, J. A. (2007). Type I interferons: something old, something new. In *Class II Cytokines* (Zdanov, A., ed.), pp. 15–49, Transworld Research Network, Kerala, India.
27. Zdanov, A. (2007). Classification and known structures of class II cytokines. In *Class II Cytokines*, pp. 1–14, Transworld Research Network, Kerala, India.
28. Yoon, S. I., Jones, B. C., Logsdon, N. J., Harris, B. D., Deshpande, A., Radaeva, S. *et al.* (2010). Structure and mechanism of receptor sharing by the IL-10R2 common chain. *Structure*, **18**, 638–648.
29. Gad, H. H., Dellgren, C., Hamming, O. J., Vends, S., Paludan, S. R. & Hartmann, R. (2009). Interferon-{lambda} is functionally an interferon but structurally related to the interleukin-10 family. *J. Biol. Chem.* **284**, 20869–20875.
30. Xu, T., Logsdon, N. J. & Walter, M. R. (2005). Structure of insect-cell-derived IL-22. *Acta Crystallogr., Sect. D: Biol. Crystallogr.* **61**, 942–950.
31. Walter, M. R. & Nagabhushan, T. L. (1995). Crystal structure of interleukin 10 reveals an interferon gamma-like fold. *Biochemistry*, **34**, 12118–12125.
32. Zdanov, A., Schalk-Hihi, C., Gustchina, A., Tsang, M., Weatherbee, J. & Wlodawer, A. (1995). Crystal structure of interleukin-10 reveals the functional dimer with an unexpected topological similarity to interferon γ. *Structure*, **3**, 591–601.
33. Zdanov, A., Schalk-Hihi, C. & Wlodawer, A. (1996). Crystal structure of human interleukin-10 at 1.6 Å resolution and a model of a complex with its soluble receptor. *Protein Sci.* **5**, 1955–1962.
34. Pletnev, S., Magracheva, E., Wlodawer, A. & Zdanov, A. (2005). A model of the ternary complex of interleukin-10 with its soluble receptors. *BMC Struct. Biol.* **5**, 10.
35. Josephson, K., Logsdon, N. J. & Walter, M. R. (2001). Crystal structure of the IL-10/IL-10R1 complex reveals a shared receptor binding site. *Immunity*, **15**, 35–46.
36. Jones, B. C., Logsdon, N. J., Josephson, K., Cook, J., Barry, P. A. & Walter, M. R. (2002). Crystal structure of human cytomegalovirus IL-10 bound to soluble human IL-10R1. *Proc. Natl Acad. Sci. USA*, **99**, 9404–9409.
37. Chang, C., Magracheva, E., Kozlov, S., Fong, S., Tobin, G., Kotenko, S. *et al.* (2003). Crystal structure of interleukin-19 defines a new subfamily of helical cytokines. *J. Biol. Chem.* **278**, 3308–3313.
38. Nagem, R. A. P., Colau, D., Dumoutier, L., Renauld, J. C., Ogata, C. & Polikarpov, I. (2002). Crystal structure of recombinant human interleukin-22. *Structure*, **10**, 1051–1062.
39. Bleicher, L., de Moura, P. R., Watanabe, L., Colau, D., Dumoutier, L., Renauld, J. C. & Polikarpov, I. (2008). Crystal structure of the IL-22/IL-22R1 complex and its implications for the IL-22 signaling mechanism. *FEBS Lett.* **582**, 2985–2992.
40. Jones, B. C., Logsdon, N. J. & Walter, M. R. (2008). Structure of IL-22 bound to its high-affinity IL-22R1 chain. *Structure*, **16**, 1333–1344.
41. de Moura, P. R., Watanabe, L., Bleicher, L., Colau, D., Dumoutier, L., Lemaire, M. M. *et al.* (2009). Crystal structure of a soluble decoy receptor IL-22BP bound to interleukin-22. *FEBS Lett.* **583**, 1072–1077.
42. Suppiah, V., Moldovan, M., Ahlenstiel, G., Berg, T., Weltman, M., Abate, M. L. *et al.* (2009). IL28B is associated with response to chronic hepatitis C interferon-alpha and ribavirin therapy. *Nat. Genet.* **41**, 1100–1104.
43. Thomas, D. L., Thio, C. L., Martin, M. P., Qi, Y., Ge, D., O'hUigin, C. *et al.* (2009). Genetic variation in IL28B and spontaneous clearance of hepatitis C virus. *Nature*, **461**, 798–801.
44. Ge, D., Fellay, J., Thompson, A. J., Simon, J. S., Shianna, K. V., Urban, T. J. *et al.* (2009). Genetic variation in IL28B predicts hepatitis C treatment-induced viral clearance. *Nature*, **461**, 399–401.
45. Thompson, A. J., Muir, A. J., Sulkowski, M. S., Ge, D., Fellay, J., Shianna, K. V. *et al.* (2010). Interleukin-28B polymorphism improves viral kinetics and is the strongest pretreatment predictor of sustained virologic response in genotype 1 hepatitis C virus. *Gastroenterology*, **139**, 120–129.
46. Tanaka, Y., Nishida, N., Sugiyama, M., Kurosaki, M., Matsuura, K., Sakamoto, N. *et al.* (2009). Genome-wide association of IL28B with response to pegylated interferon-alpha and ribavirin therapy for chronic hepatitis C. *Nat. Genet.* **41**, 1105–1109.
47. Magracheva, E., Pletnev, S., Kotenko, S., Li, W., Wlodawer, A. & Zdanov, A. (2010). Purification, crystallization and preliminary crystallographic studies of the complex of interferon-lambda1 with its receptor. *Acta Crystallogr. Sect. F: Struct. Biol. Cryst. Commun.* **66**, 61–63.
48. Presnell, S. R. & Cohen, F. E. (1989). Topological distribution of four-α-helix bundles. *Proc. Natl Acad. Sci. USA*, **86**, 6592–6596.
49. Bairoch, A., Boeckmann, B., Ferro, S. & Gasteiger, E. (2004). Swiss-Prot: juggling between evolution and stability. *Brief. Bioinform.* **5**, 39–55.
50. Leahy, D. M., Hendrickson, W. A., Aukhuil, E. & Erickson, H. P. (1992). Structure of a fibronectin type III domain from tenascin phased by MAD analysis of selenomethionyl protein. *Science*, **258**, 987–991.
51. Walter, M. R., Windsor, W. T., Nagabhushan, T. L., Lundell, D. J., Lunn, C. A., Zauodny, P. J. & Narula, S. K. (1995). Crystal structure of a complex between interferon-gamma and its soluble high-affinity receptor. *Nature*, **376**, 230–235.
52. Lawrence, M. C. & Colman, P. M. (1993). Shape complementarity at protein/protein interfaces. *J. Mol. Biol.* **234**, 946–950.
53. Josephson, K., Jones, B. C., Walter, L. J., DiGiacomo, R., Indelicato, S. R. & Walter, M. R. (2002). Noncompetitive antibody neutralization of IL-10 revealed by protein engineering and x-ray crystallography. *Structure*, **10**, 981–987.
54. Landar, A., Curry, B., Parker, M. H., DiGiacomo, R., Indelicato, S. R., Nagabhushan, T. L. *et al.* (2000). Design, characterization, and structure of a biologically active single-chain mutant of human IFN-gamma. *J. Mol. Biol.* **299**, 169–179.
55. Karpusas, M., Nolte, M., Benton, C. B., Meier, W., Lipscomb, W. N. & Goelz, S. (1997). The crystal structure of human interferon beta at 2.2-Å resolution. *Proc. Natl Acad. Sci. USA*, **94**, 11813–11818.
56. Huang, J., Smirnov, S. V., Lewis-Antes, A., Balan, M., Li, W., Tang, S. *et al.* (2007). Inhibition of type I and type III interferons by a secreted glycoprotein from Yaba-like disease virus. *Proc. Natl Acad. Sci. USA*, **104**, 9822–9827.

57. Otwinowski, Z. & Minor, W. (1997). Processing of X-ray diffraction data collected in oscillation mode. *Methods Enzymol.* **276**, 307–326.
58. McCoy, A. J. (2007). Solving structures of protein complexes by molecular replacement with Phaser. *Acta Crystallogr., Sect. D: Biol. Crystallogr.* **63**, 32–41.
59. Adams, P. D., Grosse-Kunstleve, R. W., Hung, L. W., Ioerger, T. R., McCoy, A. J., Moriarty, N. W. *et al.* (2002). PHENIX: building new software for automated crystallographic structure determination. *Acta Crystallogr. Sect. D: Biol. Crystallogr.* **58**, 1948–1954.
60. Emsley, P. & Cowtan, K. (2004). Coot: model-building tools for molecular graphics. *Acta Crystallogr. Sect. D: Biol. Crystallogr.* **60**, 2126–2132.
61. Davis, I. W., Murray, L. W., Richardson, J. S. & Richardson, D. C. (2004). MolProbity: structure validation and all-atom contact analysis for nucleic acids and their complexes. *Nucleic Acids Res.* **32**, W615–W619.
62. Berman, H. M., Westbrook, J., Feng, Z., Gilliland, G., Bhat, T. N., Weissig, H. *et al.* (2000). The Protein Data Bank. *Nucleic Acids Res.* **28**, 235–242.
63. Krissinel, E. & Henrick, K. (2007). Inference of macromolecular assemblies from crystalline state. *J. Mol. Biol.* **372**, 774–797.
64. Laskowski, R. A. (2009). PDBsum new things. *Nucleic Acids Res.* **37**, D355–D359.
65. Holm, L., Kaariainen, S., Rosenstrom, P. & Schenkel, A. (2008). Searching protein structure databases with DaliLite v.3. *Bioinformatics*, **24**, 2780–2781.
66. DeLano, W. L. (2002). *The PyMOL Molecular Graphics System.* DeLano Scientific, San Carlos, CA.